Optimization and Modeling the Processes of Green Magnetite Nanoparticle: Synthesis, Photo Catalysis Tendency and Kinetics of Removing Organic Dye from Aqueous Solutions

Avan Kareem[1] & Ibtisam Kamal[2]

[1&2] Chemical Engineering Department, Faculty of Engineering, Soran University, Kurdistan Region, Iraq
Correspondence: Avan Kareem, Chemical Engineering Department, Faculty of Engineering, Soran University, Kurdistan Region, Iraq
Email: email:avan.karem98@gmail.com

Doi: 10.23918/eajse.v9i1p71

Abstract: Green magnetite nanoparticles (NPs) are synthesized, characterized and employed for degradation Methylene Blue (MB) from aqueous solutions. The effect of the concentrations of the NPs and MB on NPs yield and removal efficiency is optimized and modeled using two factorial central composite experimental design. The analysis of variance confirmed that the concentration of iron metal salts seemed more significant than plant extract. The developed mathematical model is estimated with high R2 reflecting its accuracy. The results proved that the removal efficiency of MB increases up to an optimum of 82.07 % when using 0.17 g of the nano photo catalyst versus 10.8 ppm of MB with sunlight irradiation time of 200 min. The dye degradation kinetic results revealed that photo catalytic degradation follow pseudo-first-order model. Response Surface Methodology proved as an efficient tool for optimization and modeling the processes of NPs production and removing of organic pollutants from aqueous solutions.

Keywords: Green Magnetite Nanoparticles, Methylene Blue, Removal Efficiency, Optimization, Modeling, Metheylen Blue Degradation Rate, Removal Efficiency

1. Introduction

Among the diverse exploration of innovative aspects in the field of science and engineering, nanomaterials got immense interest across the globe including the nanoparticles due to its unique physicochemical properties, the high specific surface area and surface energy in addition to its quantum detention (Hussain et al., 2016). Nanoparticles have endless applications in different fields including industry (Klębowski et al., 2018)(Sanguansri et al., 2006)(Alanazi et al., 2010)(Maekawa et al., 2012) and environment(Salman Ali et at., 2020).

Nanoparticle could be generated following the top-down approach or bottom-up approach(Schröfel et al., 2014). Nanoparticles can be of different types, the metallic(Venkatesh et al., 2018)(Khanna et al., 2007)(X. F. Zhang et al., 2016)(Li et al., 2014)(Kim et al., 2003), metal oxide-based(Wu et al., 2008)(Chen et al., 2008)(S. Wang et al., 2019), alloy- based (Huynh et al., 2020)(J. Zhang et al., 2020)(Gilroy et al., 2016).

NPs as all nanomaterials could be synthesized through various routes (physical, chemical, and biological).

Received: October 21, 2022
Accepted: January 2, 2023
Kareem, A., & Kamal, I. (2023). Optimization and Modeling the Processes of Green Magnetite Nanoparticle: Synthesis, Photo Catalysis Tendency and Kinetics of Removing Organic Dye from Aqueous Solutions. *Eurasian Journal of Science and Engineering, 9*(1),71-88.

Physical and chemical methods are costly and toxic to the environment(Sagadevan et al., 2022) , while the biological route is an eco-friendly technique could be carried out using low energy requirements and low-costs(Pantidos et at., 2014) without using hazardous chemicals that produce toxic by-products. It involves using organisms ranging from bacteria to fungi and plants (Keat et al., 2015)(Jayaseelan et al., 2012).Plant extracts have been proposed and tested in numerous experimental works (Reverberi et al., 2017)(Gericke et al., 2006). Plants have shown potential capacity for phytoremediation of heavy metals (Iravani et al., 2011)in addition to its capability to be used as reducing agent in biosynthesis of NPs throughout its phytochemicals composition**.**

On the other hand**,** the treatment of pollutants in water and air is a great challenge. Nanomaterials confirmed its importance for the environmental remediation, they act as are excellent adsorbents, catalysts and sensors due to their high specific surface area and reactivity (Chowdhury et al., 2016)**.**

Due to the augmented development of dye industries, these industries became one of the most significant sources of organic water pollutants that enhance negative effects on the environment and human lives. In this direction several methods have been used for removing dyes from aqueous solutions, among these methods photocatalytic degradation (de Oliveira Guidolin et al., 2021)(Rajamanickam et al., 2016)(Jiang et al., 2018)are considered encouraging technologies for treating organic pollutants.

Photocatalysis implies the combination of photochemistry with catalysis(Keat et al., 2015) (Asanithi et al., 2012). Environmental remediation using photocatalysis for degradation of toxic pollutants from waste water have been studied intensively. The effect of many aspects, including catalyst concentration, pollutant concentration, solution pH, and radiation time on the kinetics (Silva et al., 2022) (Krstić et al., 2021), adsorption isotherm (Foo et al., 2010)and thermodynamics(Tripathi et al., 2019)(Elfeky et al., 2020) of pollutant degradation have been investigated. The photodegradation is a positive development to reduce waste and minimize environmental pollution (Cui et al., 2020).The situation will help to improve wastewater management at minimal cost for the highest quality of water (Anjum et al., 2019).

Different metal oxides including TiO_2, ZnO, Fe_2O_3, CdS and ZnS have been investigated as photocatalysts for degradation of organic pollutant (Jadoun et al., 2021) (Schröfel et al., 2014).In connection, the green synthesis of nanocatalyst could be of great interest to reduce the negative impact of the synthesis when toxic and hazardous chemicals are used for catalyst synthesis(Sharma et al., 2019) (Liao et al., 2004) **.**

On the other hand, Optimization is the method used to improve the performance of systems and to increase the yield of the processes without increasing the cost. Response surface methodology (RSM) is one of the efficient tools used for this purpose. It involves the use of a sequence of designed experiments to obtain an optimal response through linear models and second-degree polynomials. It is useful also for modeling and analysis of problems in which a response of interest is influenced by some variables(Ba et al., 2007) (Khoshnamvand et al., 2018) (Kumari et al., 2019) (Oehlert et al., 2000)(Amir et al., 2016)(Ngo et al., 2012). In NPs field, RSM have been used for modeling the NPS production process as well as optimization of the parameter affecting the production processes (Beg et al., 2002) (Gadekar et al., 2019) (Nikaeen et al., 2020). In addition RSM was used in optimization and modeling the removing of pollutants from waste water by absorption .(Gadekar et al., 2019)

Among the metal oxides NPs, magnetite (Fe3O4) NPs paid lot of interest owing to its low toxicity and high biocompatibility(Roy et al., 2019)(Ibañez et al., 2012)(Assa et al., 2016). In the current work, Magnetite NPs are synthesized using green route. The yield of the NPs is optimized and modeled using RSM. Methylene blue is used as a reference pollutant to evaluate the photocatalyst tendency of the prepared green NPs. MB is toxic and quite harmful when it exceeds specific concentrations, it is not biodegrade this making its removal from wastewater a challenging task (He et al., 2013)**.**In this regard, it is essential to develop effective, low-cost, and novel materials for MB and other organic dye removal from aqueous solutions.

In the current work green magnetite NPs are synthesized, characterized and used as photo catalyst to remove methylene blue dye from aqueous solutions using natural sunlight. The NPs yield and its tendency to remove MB is optimized and modeled. The kinetics and of removal are investigated and the mechanism is demonstrated.

2. Experimental Part

2.1 Raw Materials

Iron (III) chloride hexahydrate (FeCl3.6H2O) and iron (II) chloride Dihydrate (FeCl2.2H2O) Sodium hydroxide (NaOH) was purchased from Fluka. All chemicals were used without any further purification. Pomegranate peels was collected and cut to small fragments (average particle size….) and then stored in sealed containers for experimentation.

2.2 The Pollutant

MB dye was chosen as a reference pollutant for the photo catalysis experiments. Stock solutions of 100 mg/L dye were prepared with distilled water and the required concentrations were obtained by diluting.

2.3 Preparation of Green NPs

A green method was used to synthesize magnetite Fe3O4 NPs. The green approach is an eco-friendly technique to synthesis nanoparticles where it is not harmful to the human health and the environment (Patiño-Ruiz et al., 2021)(Saif et al., 2016)(Nurbas et al., 2017).The pomegranate peels were mixed with distilled water then extracted by reflux for 3 hours at 60oC. The extract was cooled then filtered twice and kept sealed at 5oC. Separately, 0.2 M iron (III) chloride hexahydrate (FeCl3.6H2O) and 0.1 M iron (II) chloride dihydrate (FeCl2.2H2O) solutions were prepared. Two factorial central composite experimental design with 10 sets of experiments was adopted to optimize and model the effect of the amounts of the plant extract (8.3-64.2) ml and the iron salts (25-66.2) ml on the yield of the NPs. The preparation procedure for all the experiments include mixing equal volumes of the iron salts solutions and the plant extract. The pH of the mixture was then adjusted to 11-11.5 by adding the freshly prepared 1.0 M of NaOH drop-wise to the solution while constant stirring continuously. After that, the solution stirred on a hot plate at 60℃ for 1 h for the completion of the reaction. The creation of Fe3O4 nanoparticles was confirmed by altering the color of the mixed solution from light brown to dark black. The prepared NPs were purified by washing three times with Ethanol, the pure solid NPs were dried in an oven at 100 °C for 24 h. Then, the dried NPs were used for characterization. Table 1 shows the adopted experimental design for magnetite NPs preparation.

Table 1: The actual levels for the operating variables used for preparation the green magnetite NPs.

Exp. No.	1*	2	3	4	5	6	7	8	9
Plant extract (ml)	25.0	10.0	64.2	8.3	40.0	25.0	10.0	40.0	23.8
Fe salts (ml)	45.0	60.0	45.0	45.0	60.0	66.2	30.0	30.0	25.0
NPs yield (g)	2.9	3.3	4.0	3.2	5.0	3.9	2.5	3.1	1.0

*repetitions

2.4 Photo Catalysis Experiments

The photo catalysis experiments were carried out to evaluate the photo catalysis performance of the green prepared NPs. The photo calysis experiments were completed based on the experimental design illustrated in Table 2. The effect of the photo catalyst (Green NPs) dose (0.03-0.17) g and MB concentration (2.9-17) mg/l on removal efficiency was investigated.

Table 2: Experimental design, actual levels of the operating variables

Exp. No.	1	2	3	4	5	6	7*	8	9
Catalyst dose (g)	0.17	0.1	0.05	0.15	0.05	0.1	0.1	0.15	0.03
MB concentration (ppm)	10	17	5	5	15	2.9	10	15	10
Removal efficiency % (Irradiation time=200min.)	85	69	32	55	58	18	76	61	72

*repetitions

25 ml of different initial concentrations of MB solutions were added to the predetermined amount of NPs (photo catalyst). The sealed mixtures were exposed to sunlight during continuous stirring at 300 rpm. The aqueous samples were taken at pre-set time intervals, filtered and their concentrations were determined by UV-6100A spectrophotometer at the maximum absorption wavelength of 664 nm. The removal efficiency was calculated based on an adopted calibration curve for MB (Figure 1) which explains the relation between absorbance and the concentrations of MB solutions prepared by using eight successive concentrations from MB for range between 2-17 mg/L.

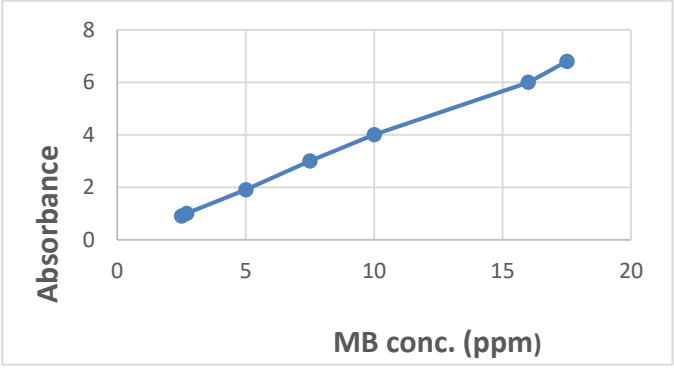

Figure 1: MB calibration curve

The removal efficiency was calculated using the following equation:

$$\% \text{ Removal} = (Co - Ct/Co) \times 100 \quad [1]$$

Where Co= Initial concentration of MB (mg/L) and Ct= concentration of MB (mg/L) at time t.

On another hand, The MB degradation mode under the photo catalysis for each experiment was identified by plotting the ratio of the concentration of MB at any sunlight exposure time to its initial (C/Co) against the irradiation time. In addition, the degradation rate at certain time qt (ppm/g) was calculated for all the experiments for the samples sunlight irradiated after100 and 200 min. using the following equation:

$$qt = V\,(Co - Ct)/m \quad [2]$$

Where Co= Initial concentration of MB (mg/L) and Ct= MB concentration (mg/L) at time t.

The dye degradation kinetic data are adjusted by the adapted models of pseudo-first-order and pseudo-second-order.

3. Results and Discussion

3.1 Characterization of the Green Magnetite Fe3O4 Nanoparticles

The prepared magnetite Fe3O4 NPs were characterized by UV-VIS spectroscopy, scanning electron microscopy (SEM), Energy Dispersive X-ray (EDX) and (TEM). The optical properties and band gap in the 200–700 nm wavelength range were studied with a UV-Vis spectrophotometer. The geometry and morphology of Fe3O4 NPs were investigated using SEM and TEM.

Figure 2 shows the characterization techniques and the results of a typical sample of green magnetite NPs. Figure 2a show the UV-Visible spectra of Fe3O4 nanoparticles biosynthesized using pomegranate peels extract. The result showed a maximum absorption peak around 350 nm; this indicates the formation of Fe3O4 NPs. Similar UV results for magnetite NPs were found in literature(Yew et al., 2016)(Abdallah et al., 2021)(Sathishkumar et al., 2018).

Figure 2b and 2c shows the Scanning electron microscopy (SEM) and TEM images Fe3O4 NPs respectively. The SEM image shows that the NPs are with spherical, cubic-like shape with remarkable agglomerate morphologies. Figure 2d shows the particle size distribution of Fe3O4 NPs. The particles have a narrow size range, with a mean average size of 113 nm.

Regarding the elemental composition, the Energy Dispersive X-ray (EDX) plot shows that iron and oxygen are the primary components of the NPs structures.

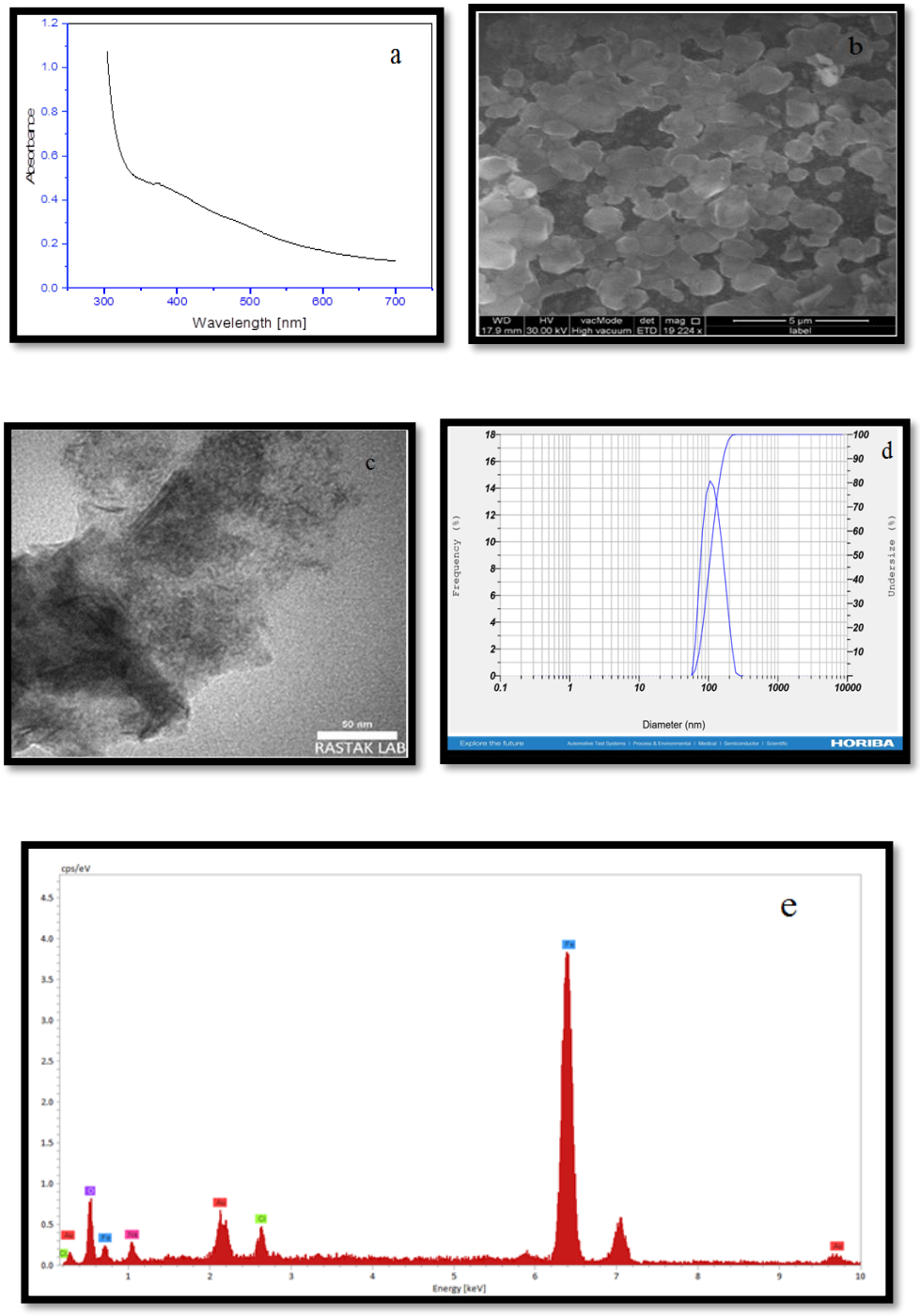

Figure 2: Characterization of Fe_3O_4 NPs. a: UV spectra, b: SEM image, c: TEM image, d: Particle size distribution, e: Energy Dispersive X-ray (EDX) image

3.2 MB Degradation Mode and Rate and Removal Efficiency

The MB degradation mode under the photo catalysis process is illustrated by plotting the ratio of the concentration of MB at any sunlight exposure time to its initial (C/Co) for each experiment against the irradiation time. Typical plots are seen in Figure 3.

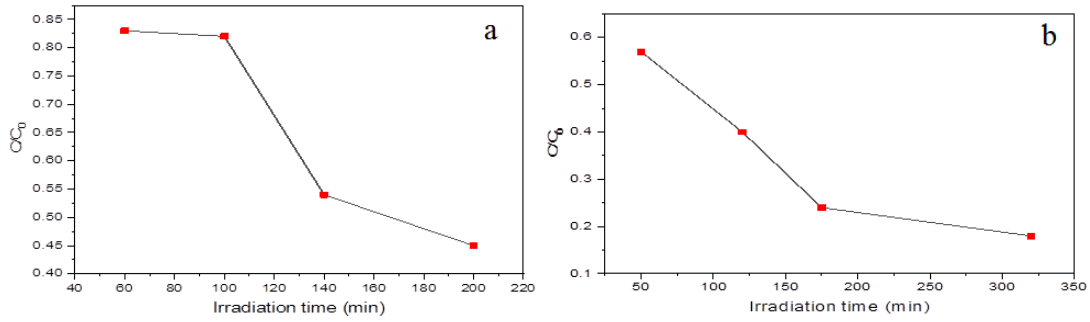

Figure 3: Mode and profile of Photolytic degradation of MB using green Magnetite NPs. (a): Exp.no.4, (b): Exp. No. 7.

It is obvious to note that the photo degradation of the dye increases with increasing sunlight irradiation time. It can be seen that the degradation ratio significantly decreased with the increasing the irradiation time during the initial degradation time and then remained decrease but with lower rate. The situation may be attributed to that at the beginning of degradation, a large number of active sites on the surface of NPs could be used, causing a fast degradation rate. However, more and more active sites became occupied by the MB molecules with the increasing irradiation time. Furthermore, a strong repulsive force may be generated between the degraded MB ions and the undegraded MB ions, making the remaining sites more and more difficult to occupy. However, the inflection point varies for each experiment. This indicates that both the concentration of the photo catalyst and MB had an obvious effect on the degradation ratio of MB. During the beginning of degradation, the larger the MB concentration, the more the contact chance between the MB molecules and NPs, resulting in a higher degradation rate. The enhanced photocatalytic activity may be related to the synergetic adsorption–photocatalytic degradation effect of the green NPs. After a certain sunlight exposure time, the MB degradation moves to a steady state. An increasing MB concentration will increase the driving force for the photo catalysis and, of course, would promote the degradation. The phenomena were highly approved by plotting the degradation rate at certain time qt (ppm/g) versus the concentration of MB at constant catalyst dose.

Figure 4a shows that at constant dose of the photo catalyst (0.1g), the rate of degradation at 100 min and 200 min increases with increasing the concentration of MB. Nevertheless, the degradation rate is affected by both the concentration of MB and the photo catalyst dose as illustrated in Figure 4b.

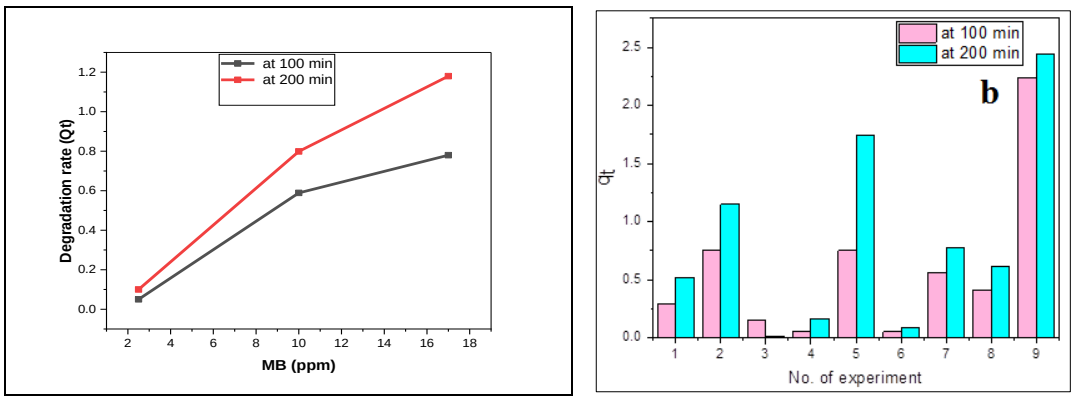

Figure 4: (a): MB degradation rate versus concentration at constant photo catalyst dose, (b): Degradation rate at sunlight exposure for 100 and 200 min. versus the designed experiments.

The removal efficiency showed the same trend as shown in Figure 5.

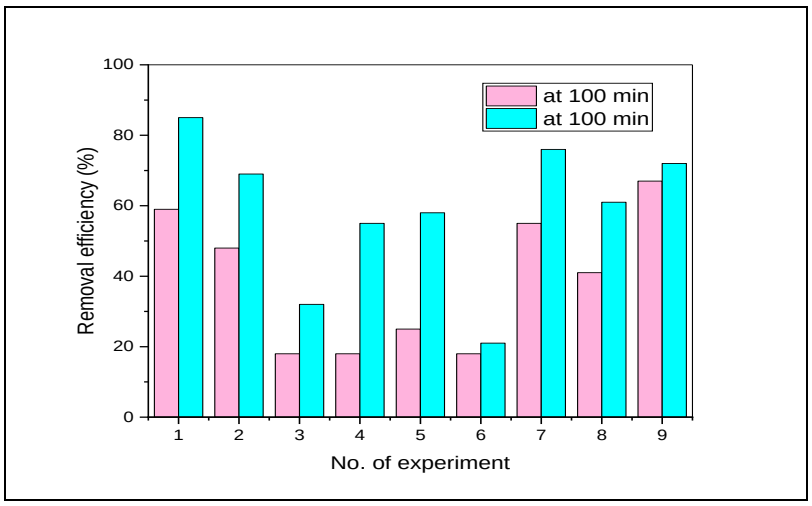

Figure 5: Removal efficiency % versus no. of experiments.

The MB molecules, will gain a positive charge after dissolution in water, will be degraded more and faster with a subsequent increase in the percentage color removal.

3.3 ANOVA Results for MB Degradation Rate and the Removal Efficiency of the Photo Catalyst

In this work the central composite design (CCD) approach of RSM was used based on two independent variables (the volume of pomegranate extract and the volume of the Fe salts). Ten different experiments were developed including six volume levels of plant extract (8.3, 10.0, 23.8, 25.0, 40.0 and 64.2) ml and five volume levels of the solutions of Fe salts concentration (25.0, 30, 45.0,60.0 and 66.2) ml.

The Pareto chart was established to examine the absolute magnitude, importance, and interactions of the standard effects of the two independent variables on the green NPs yield. Figure 6a showed that the two operating variables are significant reflecting by drawing the reference line on the graph, however, the volume of Fe salts seemed more significant. The positive sign of the effects of the two factors indicated that the NPs yield increases with increasing the volumes of the two variables. Figure 6b justified the effects. The 3D response surface of the effect of the two variables is shown in figure 6c, while the non-oval-shaped contour estimated response surface lines in Figure 6d predicts that there is no interaction between the factors and the response. The former situation is justified by parallel lines of the interaction plots of Figure 6e. The experimental data have been analyzed to evaluate the normality of actual values versus predicted for NPs yield. Figure 6f shows the normal probability plot which indicates that all the plotted points for the NPs yield are very close to the fitted distribution line which reflected that the experimental data were in good correlation with the predicted model outcomes, thus the generated response model is applicable and acceptable for estimating the NPs yield

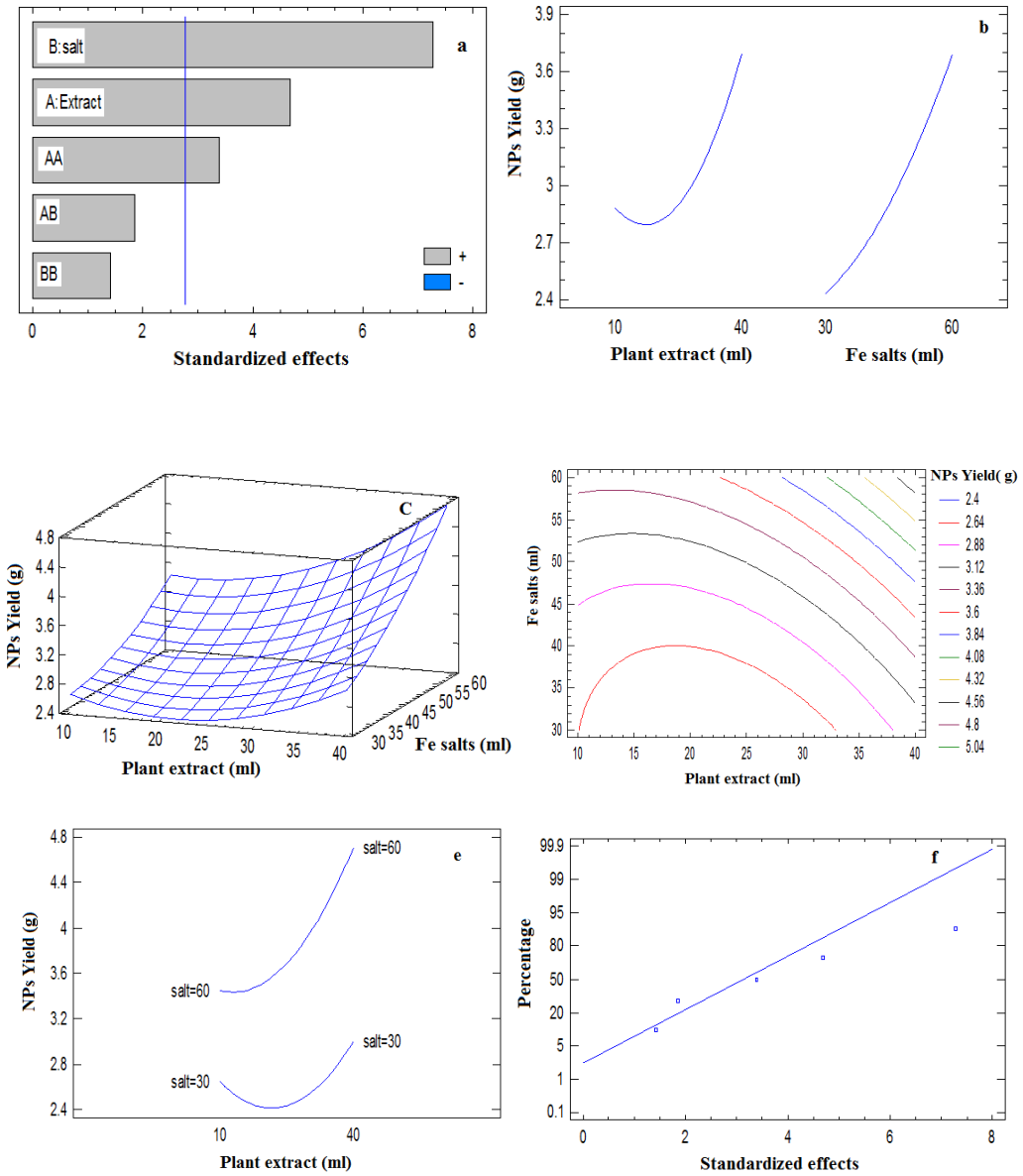

Figure 6. Pareto chart (a), standardized effects plot (b). 3-D estimated response surface (c), 2-D counter plots (d), Interaction plots (e), Normal probability plot (f) for NPs yield.

The results of the analysis of variance (ANOVA) performed on NPs yield resulted in the following mathematical model:

$$\text{NPs Yield (g)} = 4.01 - 0.104*E - 0.05*S + 0.002*E^{\wedge 2} + 0.001*E*S + 0.001*S^{\wedge 2} \quad [3]$$

Where E is the plant extract volume (ml)and S is the volume of Fe salts (ml).

The polynomial estimated with a P-values <0.05 that imply the model and parameter are significant and the developed model is of high accuracy. The model's fitness and adequacy is reflected by the computed high coefficients of determination (R2) = 95.75 % and adjusted coefficients (R2adj) =90.41 %. which indicate the models' predictive capacity?

The model was estimated with optimum NPs yield of 5.91 g produced from the reaction of 46.21 ml of plant extract with 66.21 ml of each Fe salt.

The ANOVA results for removal efficiency of the photo catalyst (NPs) for MB are illustrated in Figure 8. The Pareto chart (figure 8a) showed that MB concentration has the top significant effect compared to the photo catalyst, however, the removal efficiency increases with increasing the amount of the photo catalyst and MB, but regarding the MB it increases to an optimum level then decreases as illustrated in Figure 8b. The reason may be attributed to decreasing the number of active sites on the surface of NPs as more active sites became occupied by the MB molecules.

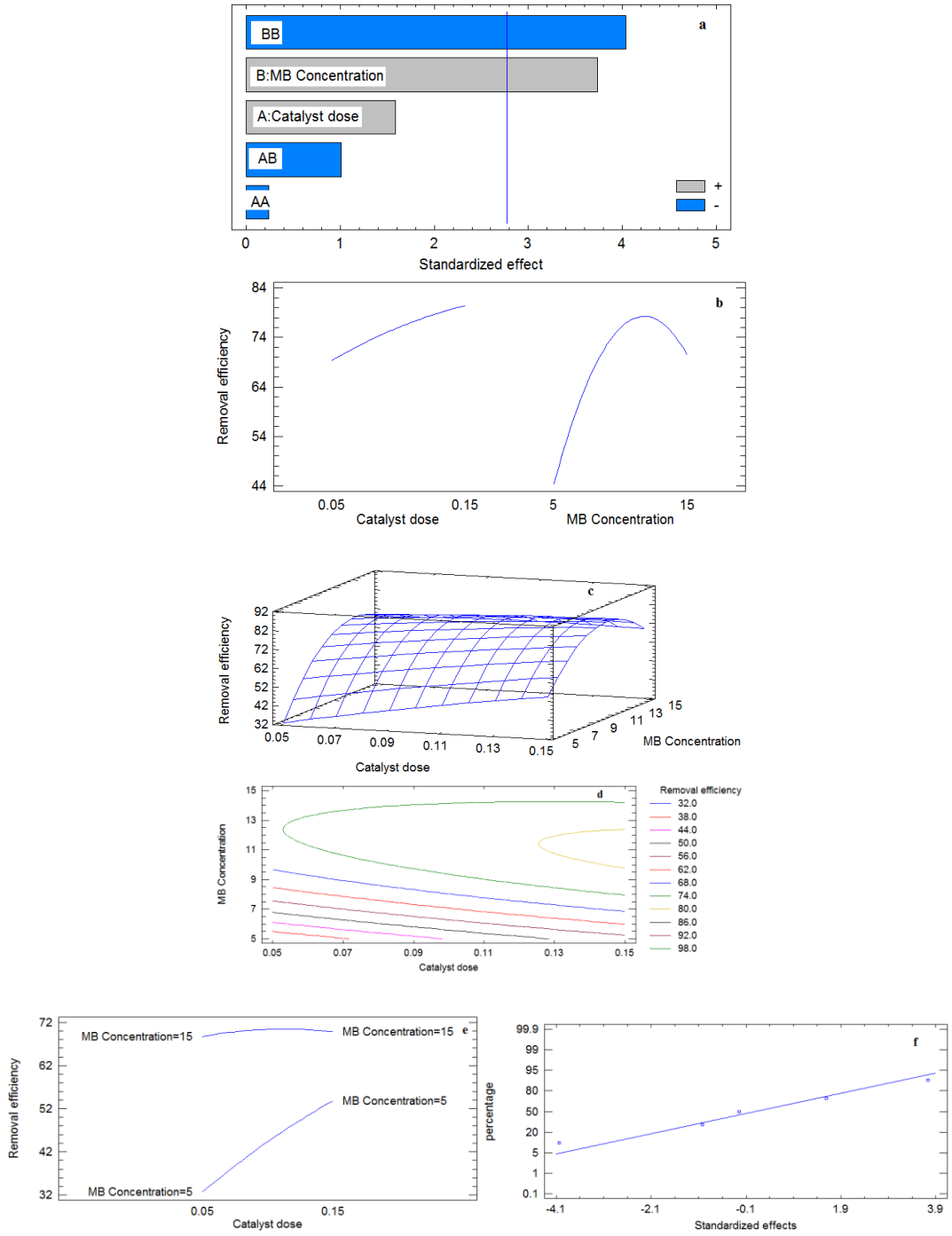

Figure 7: Pareto chart (a), standardized effects plot (b). 3-D estimated response surface (c), 2-D counter plots (d), Interaction plots (e), Normal probability plot (f) for removal efficiency.

The effect of the load of the photo catalyst and the concentration of MB is obvious in the 3D-estimated response surface plot (Figure 8c). The non-interaction effect of the operating variables with the response is clarified in the non-oval-shaped contour response surface lines in Figure 8d and the parallel lines of the interaction plots in Figure 8e. The normal probability plot showed that all the plotted points for the removal efficiency are close-fitting to the distribution line which indicated the high tendency of the generated model to explain the experimental results

The generated mathematical model is described in the following polynomial equation:

$$\text{Removal efficiency \%} = -60.13 + 40.10*C + 19.50*M - 4.5*C^2 - 2.0*C*M - 0.75*M^2 \quad [4]$$

Where C is the photo catalyst (g). M is the MC conc.(mg/l)).

The model's fitness and adequacy is approved such as the polynomial estimated is with a P-values <0.05 and high coefficients of determination (R2) = 90.13 %.

The optimum removal efficiency % estimated by the model is 82.07 could be reached with an optimum photo catalyst load of 0.17 g and 10.8 mg/l MB.

3.4 Effect of pH on Removal Efficiency

The effect of pH on removal efficiency of MB by the photo catalyst was studied by using the optimum catalyst dose (0.17g) and MB concentration (10.8 mg/l) estimated from ANOVA at different pH (3,5,7,9 and 11.2). NaOH (0.1N) and HCl (0.1N) were used to adjust the pH. The pH was measured by using pH-meter. The pH is the important factor which controls the removal process of the dyes (Yaseen & Scholz, 2019)(Gutiérrez et al., 2001)(Hashim et al., 2019).As elucidated in Figure 8 shown effect of various PH in removal efficiency. the dye removal was minimum at pH 3, but it increased as the pH was increased from 2 to 11.2. The situation is attributed to that at low pH, the dye become protonated. The neutralization of the negative charges at the surface of the catalyst cause a decrease in the removal efficiency in the acidic media owing to the electrostatic repulsion between the protonated dyes and positively charged photo catalyst sites. Increasing the pH will facilitate the diffusion process and provides more active sites (negative charge groups) at the surface of the catalyst thus facilitating greater dye removal. Similar trends were observed in the literature (Nguyen & Fogler, 2005)(Gros et al., 1976).

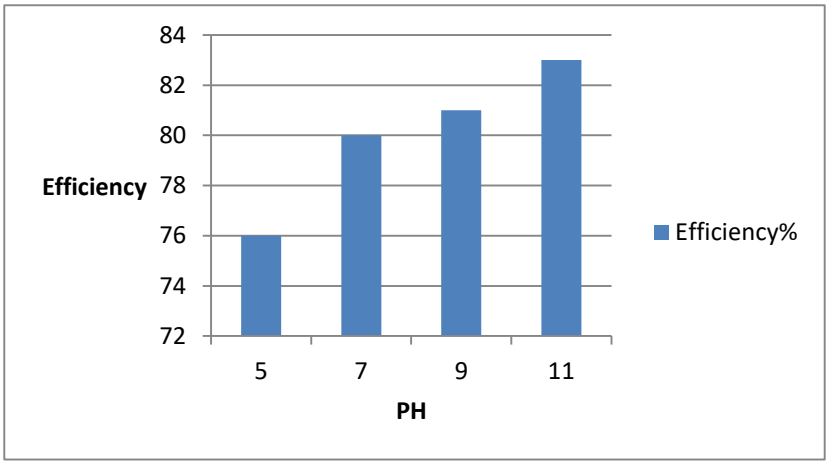

Figure 8: removal efficiency % in versus no. of PH (9,7,5).

3.5 MB Degradation Kinetics

Kinetics study is important to the photo catalysis process because it depicts the degradation rate and adsorption of pollutant and controls the residual time of the whole photo catalysis process (J. Wang et al., 2017)(Giovannetti et al., 2016)(Kurajica et al., 2018)To explore the kinetics of the photo catalysis process, the experimental data were fitted to the pseudo-first-order, pseudo-second-order, and intraparticle diffusion models.

The linear forms of the pseudo-first-order and the pseudo-second-order are represented by:

$$\ln(q_e - q_t) = \ln q_e - \mathrm{K1}\ t \quad [5]$$

$$\frac{t}{q_t} = \frac{1}{K_2 q_e^2} + \frac{t}{q_e} \quad [6]$$

where K 1 (min−1) and K 2 (g·mg−1·min−1) are the rate constants of the pseudo-first-order and pseudo-second-order, respectively.

The pseudo-first-order kinetic model is based on the assumption that the adsorption process of MB molecules is the physical adsorption. The second-order model is based on the assumption that the adsorption process is the chemical adsorption. The parameters of kinetic models and the correlation coefficient (R 2) values were obtained by linear regression. They are listed in Table 3.

Table 3: The parameters of the kinetic models estimated.

		Pseudo- first order			Pseudo-second order		
C_0 (mg/l)	Time (min)	q_e mg/g	K_1 min^{-1}	R^2	q_e mg/g	K_2 min^{-1}	R^2
4.05	60	15.788	0.011	0.97	16.99	0.0259	0.83
	120	16.67	0.00835		16.18	0.0274	
	140	16.8	0.00845		16.85	0.0276	
	160	16.9	0.0107		16.90	0.462	

As can be seen, the R 2 values obtained from the pseudo-first-order were consistently higher than those from the pseudo-second-order. In addition, the qe values coincided with the expected qe values (qe, exp). That indicates that the adsorption of MB molecules and its degradation perfectly obeys the pseudo-second-order model meaning the controlling rate step is chemisorption (Vasiljevic et al., 2020)(Xu et al., 2014)(Kundu et al., 2019).

4. Conclusions

Magnetite NPs synthesized by plant mediated method is a cost effective, safe and ecofriendly nanomaterials have unique optical and photo catalysis properties that highly candidate them for environmental remediation including degradation of organic dyes pollutant such as MB from aqueous solutions as well as wastewater. The optimization of the synthesis process revealed that both plant extract concentration and the metal salts have significant effect of the yield of NPs, however the metal

salt concentration seemed more significant. Also, the rate of adsorption and degradation of the dye increases with increasing the concentration of dye. The parameters of kinetic models confirmed that the adsorption of MB molecules and its degradation perfectly obeys the pseudo-first-order model meaning the controlling rate step is chemisorption rather than physical adsorption.

References

Abdallah, R. M., & Al-Haddad, R. M. S. (2021). Optical and Morphology Properties of the Magnetite (Fe3O4) Nanoparticles Prepared by Green Method. *Journal of Physics: Conference Series*, *1829*(1). https://doi.org/10.1088/1742-6596/1829/1/012022

Alanazi, F. K., Radwan, A. A., & Alsarra, I. A. (2010). Biopharmaceutical applications of nanogold. *Saudi Pharmaceutical Journal*, *18*(4), 179–193. https://doi.org/10.1016/j.jsps.2010.07.002

Amir, W. M., Shafiq, M., Mokhtar, K., Aleng, N. A., Rahim, H. A., & Ali, Z. (2016). JMASM algorithms and code simple response surface methodology using RSREG (SAS). *Journal of Modern Applied Statistical Methods*, *15*(1), 855–867. https://doi.org/10.22237/jmasm/1462077780

Anjum, M., Miandad, R., Waqas, M., Gehany, F., & Barakat, M. A. (2019). Remediation of wastewater using various nano-materials. *Arabian Journal of Chemistry*, *12*(8), 4897–4919. https://doi.org/10.1016/j.arabjc.2016.10.004

Asanithi, P., Chaiyakun, S., & Limsuwan, P. (2012). Growth of silver nanoparticles by DC magnetron sputtering. *Journal of Nanomaterials*, *2012*. https://doi.org/10.1155/2012/963609

Assa, F., Jafarizadeh-Malmiri, H., Ajamein, H., Anarjan, N., Vaghari, H., Sayyar, Z., & Berenjian, A. (2016). A biotechnological perspective on the application of iron oxide nanoparticles. *Nano Research*, *9*(8), 2203–2225. https://doi.org/10.1007/s12274-016-1131-9

Ba, D., & Boyaci, I. H. (2007). Modeling and optimization i: Usability of response surface methodology. *Journal of Food Engineering*, *78*(3), 836–845. https://doi.org/10.1016/j.jfoodeng.2005.11.024

Beg, Q. K., Saxena, R. K., & Gupta, R. (2002). Kinetic constants determination for an alkaline protease from Bacillus mojavensis using response surface methodology. *Biotechnology and Bioengineering*, *78*(3), 289–295. https://doi.org/10.1002/bit.10203

Chen, L., Yokel, R. A., Hennig, B., & Toborek, M. (2008). Manufactured aluminum oxide nanoparticles decrease expression of tight junction proteins in brain vasculature. *Journal of Neuroimmune Pharmacology*, *3*(4), 286–295. https://doi.org/10.1007/s11481-008-9131-5

Chowdhury, S., Yusof, F., Faruck, M. O., & Sulaiman, N. (2016). Process Optimization of Silver Nanoparticle Synthesis Using Response Surface Methodology. *Procedia Engineering*, *148*, 992–999. https://doi.org/10.1016/j.proeng.2016.06.552

Cui, J., Zhang, F., Li, H., Cui, J., Ren, Y., & Yu, X. (2020). Recent progress in biochar-based photocatalysts for wastewater treatment: Synthesis, mechanisms, and applications. *Applied Sciences (Switzerland)*, *10*(3). https://doi.org/10.3390/app10031019

de Oliveira Guidolin, T., Possolli, N. M., Polla, M. B., Wermuth, T. B., Franco de Oliveira, T., Eller, S., Klegues Montedo, O. R., Arcaro, S., & Cechinel, M. A. P. (2021). Photocatalytic pathway on the degradation of methylene blue from aqueous solutions using magnetite nanoparticles. *Journal of Cleaner Production*, *318*(August). https://doi.org/10.1016/j.jclepro.2021.128556

Elfeky, A. S., Youssef, H. F., & Elzaref, A. S. (2020). Adsorption of Dye from Wastewater onto ZnO Nanoparticles-Loaded Zeolite: Kinetic, Thermodynamic and Isotherm Studies.

Zeitschrift Fur Physikalische Chemie, *234*(2), 255–278. https://doi.org/10.1515/zpch-2018-1342

Foo, K. Y., & Hameed, B. H. (2010). Insights into the modeling of adsorption isotherm systems. *Chemical Engineering Journal*, *156*(1), 2–10. https://doi.org/10.1016/j.cej.2009.09.013

Gadekar, M. R., & Ahammed, M. M. (2019). Modelling dye removal by adsorption onto water treatment residuals using combined response surface methodology-artificial neural network approach. *Journal of Environmental Management*, *231*(April 2018), 241–248. https://doi.org/10.1016/j.jenvman.2018.10.017

Gericke, M., & Pinches, A. (2006). Microbial production of gold nanoparticles. *Gold Bulletin*, *39*(1), 22–28. https://doi.org/10.1007/BF03215529

Gilroy, K. D., Ruditskiy, A., Peng, H. C., Qin, D., & Xia, Y. (2016). Bimetallic nanocrystals: Syntheses, properties, and applications. *Chemical Reviews*, *116*(18), 10414–10472. https://doi.org/10.1021/acs.chemrev.6b00211

Giovannetti, R., Rommozzi, E., D'Amato, C. A., & Zannotti, M. (2016). Kinetic model for simultaneous adsorption/photodegradation process of alizarin red S in water solution by nano-TiO2 under visible light. *Catalysts*, *6*(6). https://doi.org/10.3390/catal6060084

Gros, G., Moll, W., Hoppe, H., & Gros, H. (1976). Proton transport by phosphate diffusion - a mechanism of facilitated CO2 transfer. *Journal of General Physiology*, *67*(6), 773–790. https://doi.org/10.1085/jgp.67.6.773

Gutiérrez, M. C., Pepió, M., Crespi, M., & Mayor, N. (2001). Control factors in the electrochemical oxidation of reactive dyes. *Coloration Technology*, *117*(6), 356–361. https://doi.org/10.1111/j.1478-4408.2001.tb00090.x

Hashim, K. S., Hussein, A. H., Zubaidi, S. L., Kot, P., Kraidi, L., Alkhaddar, R., Shaw, A., & Alwash, R. (2019). Effect of initial pH value on the removal of reactive black dye from water by electrocoagulation (EC) method. *Journal of Physics: Conference Series*, *1294*(7). https://doi.org/10.1088/1742-6596/1294/7/072017

He, X., Male, K. B., Nesterenko, P. N., Brabazon, D., Paull, B., & Luong, J. H. T. (2013). Adsorption and desorption of methylene blue on porous carbon monoliths and nanocrystalline cellulose. *ACS Applied Materials and Interfaces*, *5*(17), 8796–8804. https://doi.org/10.1021/am403222u

Hussain, I., Singh, N. B., Singh, A., Singh, H., & Singh, S. C. (2016). Green synthesis of nanoparticles and its potential application. *Biotechnology Letters*, *38*(4), 545–560. https://doi.org/10.1007/s10529-015-2026-7

Huynh, K. H., Pham, X. H., Kim, J., Lee, S. H., Chang, H., Rho, W. Y., & Jun, B. H. (2020). Synthesis, properties, and biological applications of metallic alloy nanoparticles. *International Journal of Molecular Sciences*, *21*(14), 1–29. https://doi.org/10.3390/ijms21145174

Ibañez, F. J., & Zamborini, F. P. (2012). Chemiresistive sensing with chemically modified metal and alloy nanoparticles. *Small*, *8*(2), 174–202. https://doi.org/10.1002/smll.201002232

Iravani, S. (2011). Green synthesis of metal nanoparticles using plants. *Green Chemistry*, *13*(10), 2638–2650. https://doi.org/10.1039/c1gc15386b

Jadoun, S., Arif, R., Jangid, N. K., & Meena, R. K. (2021). Green synthesis of nanoparticles using plant extracts: a review. *Environmental Chemistry Letters*, *19*(1), 355–374. https://doi.org/10.1007/s10311-020-01074-x

Jayaseelan, C., Rahuman, A. A., Kirthi, A. V., Marimuthu, S., Santhoshkumar, T., Bagavan, A., Gaurav, K., Karthik, L., & Rao, K. V. B. (2012). Novel microbial route to synthesize ZnO

nanoparticles using Aeromonas hydrophila and their activity against pathogenic bacteria and fungi. *Spectrochimica Acta - Part A: Molecular and Biomolecular Spectroscopy*, *90*, 78–84. https://doi.org/10.1016/j.saa.2012.01.006

Jiang, X. H., Wang, L. C., Yu, F., Nie, Y. C., Xing, Q. J., Liu, X., Pei, Y., Zou, J. P., & Dai, W. L. (2018). Photodegradation of Organic Pollutants Coupled with Simultaneous Photocatalytic Evolution of Hydrogen Using Quantum-Dot-Modified g-C3N4 Catalysts under Visible-Light Irradiation. *ACS Sustainable Chemistry and Engineering*, *6*(10), 12695–12705. https://doi.org/10.1021/acssuschemeng.8b01695

Keat, C. L., Aziz, A., Eid, A. M., & Elmarzugi, N. A. (2015). Biosynthesis of nanoparticles and silver nanoparticles. *Bioresources and Bioprocessing*, *2*(1). https://doi.org/10.1186/s40643-015-0076-2

Khanna, P. K., Gaikwad, S., Adhyapak, P. V., Singh, N., & Marimuthu, R. (2007). Synthesis and characterization of copper nanoparticles. *Materials Letters*, *61*(25), 4711–4714. https://doi.org/10.1016/j.matlet.2007.03.014

Khoshnamvand, N., Kord Mostafapour, F., Mohammadi, A., & Faraji, M. (2018). Response surface methodology (RSM) modeling to improve removal of ciprofloxacin from aqueous solutions in photocatalytic process using copper oxide nanoparticles (CuO/UV). *AMB Express*, *8*(1), 0–8. https://doi.org/10.1186/s13568-018-0579-2

Kim, S. W., Park, J., Jang, Y., Chung, Y., Hwang, S., Hyeon, T., & Kim, Y. W. (2003). Synthesis of monodisperse palladium nanoparticles. *Nano Letters*, *3*(9), 1289–1291. https://doi.org/10.1021/nl0343405

Klębowski, B., Depciuch, J., Parlińska-Wojtan, M., & Baran, J. (2018). Applications of noble metal-based nanoparticles in medicine. *International Journal of Molecular Sciences*, *19*(12). https://doi.org/10.3390/ijms19124031

Krstić, V. (2021). Role of zeolite adsorbent in water treatment. In *Handbook of Nanomaterials for Wastewater Treatment*. https://doi.org/10.1016/b978-0-12-821496-1.00024-6

Kumari, M., & Gupta, S. K. (2019). Response surface methodological (RSM) approach for optimizing the removal of trihalomethanes (THMs) and its precursor's by surfactant modified magnetic nanoadsorbents (sMNP) - An endeavor to diminish probable cancer risk. *Scientific Reports*, *9*(1), 1–11. https://doi.org/10.1038/s41598-019-54902-8

Kundu, A., & Mondal, A. (2019). Photodegradation of methylene blue under direct sunbeams by synthesized anatase titania nanoparticles. *SN Applied Sciences*, *1*(3). https://doi.org/10.1007/s42452-019-0280-3

Kurajica, S., Minga, I., Blazic, R., Muzina, K., & Tominac, P. (2018). Adsorption and Degradation Kinetics of Methylene Blue on As-prepared and Calcined Titanate Nanotubes. *Athens Journal of Sciences*, *5*(1), 7–22. https://doi.org/10.30958/ajs.5-1-1

Li, N., Zhao, P., & Astruc, D. (2014). Anisotropic gold nanoparticles: Synthesis, properties, applications, and toxicity. *Angewandte Chemie - International Edition*, *53*(7), 1756–1789. https://doi.org/10.1002/anie.201300441

Liao, S., Donggen, H., Yu, D., Su, Y., & Yuan, G. (2004). Preparation and characterization of ZnO/TiO2, SO42-/ZnO/TiO2 photocatalyst and their photocatalysis. *Journal of Photochemistry and Photobiology A: Chemistry*, *168*(1–2), 7–13. https://doi.org/10.1016/j.jphotochem.2004.05.010

Madkour, L. H. (2019). Polymer nanoparticle drug-nucleic acid combinations. *Nucleic Acids as Gene Anticancer Drug Delivery Therapy*, 241–255. https://doi.org/10.1016/b978-0-12-819777-6.00014-7

Maekawa, K., Yamasaki, K., Niizeki, T., Mita, M., Matsuba, Y., Terada, N., & Saito, H. (2012). Drop-on-demand laser sintering with silver nanoparticles for electronics packaging. *IEEE Transactions on Components, Packaging and Manufacturing Technology*, *2*(5), 868–877. https://doi.org/10.1109/TCPMT.2011.2178606

Ngo, Hoang, T. (2012). The Steps to Follow in a Multiple Regression Analysis. *SAS Global Forum 2012*, 1–12.

Nguyen, D. A., & Fogler, H. S. (2005). Facilitated diffusion in the dissolution of carboxylic polymers. *AIChE Journal*, *51*(2), 415–425. https://doi.org/10.1002/aic.10329

Nikaeen, G., Yousefinejad, S., Rahmdel, S., Samari, F., & Mahdavinia, S. (2020). Central Composite Design for Optimizing the Biosynthesis of Silver Nanoparticles using Plantago major Extract and Investigating Antibacterial, Antifungal and Antioxidant Activity. *Scientific Reports*, *10*(1), 1–16. https://doi.org/10.1038/s41598-020-66357-3

Nurbas, M., Ghorbanpoor, H., & Avci, H. (2017). An eco-friendly approach to synthesis and characterization of magnetite (Fe3O4) nanoparticles using Platanus Orientalis L. leaf extract. *Digest Journal of Nanomaterials and Biostructures*, *12*(4), 993–1000.

Oehlert, G. W. (2000). A First Course in Design and Analysis of Experiments. In *The American Statistician* (Vol. 1, Issue 1). http://users.stat.umn.edu/~gary/book/fcdae.pdf

Pantidos, N. (2014). Biological Synthesis of Metallic Nanoparticles by Bacteria, Fungi and Plants. *Journal of Nanomedicine & Nanotechnology*, *05*(05). https://doi.org/10.4172/2157-7439.1000233

Patiño-Ruiz, D. A., Meramo-Hurtado, S. I., González-Delgado, Á. D., & Herrera, A. (2021). Environmental Sustainability Evaluation of Iron Oxide Nanoparticles Synthesized via Green Synthesis and the Coprecipitation Method: A Comparative Life Cycle Assessment Study. *ACS Omega*, *6*(19), 12410–12423. https://doi.org/10.1021/acsomega.0c05246

Rajamanickam, D., & Shanthi, M. (2016). Photocatalytic degradation of an organic pollutant by zinc oxide – solar process. *Arabian Journal of Chemistry*, *9*, S1858–S1868. https://doi.org/10.1016/j.arabjc.2012.05.006

Reverberi, A. P., Vocciante, M., Lunghi, E., Pietrelli, L., & Fabiano, B. (2017). New trends in the synthesis of nanoparticles by green methods. *Chemical Engineering Transactions*, *61*, 667–672. https://doi.org/10.3303/CET1761109

Roy, A., Bulut, O., Some, S., Mandal, A. K., & Yilmaz, M. D. (2019). Green synthesis of silver nanoparticles: Biomolecule-nanoparticle organizations targeting antimicrobial activity. *RSC Advances*, *9*(5), 2673–2702. https://doi.org/10.1039/c8ra08982e

Sagadevan, S., Imteyaz, S., Murugan, B., Anita Lett, J., Sridewi, N., Weldegebrieal, G. K., Fatimah, I., & Oh, W. C. (2022). A comprehensive review on green synthesis of titanium dioxide nanoparticles and their diverse biomedical applications. *Green Processing and Synthesis*, *11*(1), 44–63. https://doi.org/10.1515/gps-2022-0005

Saif, S., Tahir, A., & Chen, Y. (2016). Green synthesis of iron nanoparticles and their environmental applications and implications. *Nanomaterials*, *6*(11), 1–26. https://doi.org/10.3390/nano6110209

Salman Ali, A. (2020). Application of Nanomaterials in Environmental Improvement. *Nanotechnology and the Environment*, 1–20. https://doi.org/10.5772/intechopen.91438

Sanguansri, P., & Augustin, M. A. (2006). Nanoscale materials development - a food industry perspective. *Trends in Food Science and Technology*, *17*(10), 547–556. https://doi.org/10.1016/j.tifs.2006.04.010

Sathishkumar, G., Logeshwaran, V., Sarathbabu, S., Jha, P. K., Jeyaraj, M., Rajkuberan, C., Senthilkumar, N., & Sivaramakrishnan, S. (2018). Green synthesis of magnetic Fe3O4 nanoparticles using Couroupita guianensis Aubl. fruit extract for their antibacterial and cytotoxicity activities. *Artificial Cells, Nanomedicine and Biotechnology*, *46*(3), 589–598. https://doi.org/10.1080/21691401.2017.1332635

Schröfel, A., Kratošová, G., Šafařík, I., Šafaříková, M., Raška, I., & Shor, L. M. (2014). Applications of biosynthesized metallic nanoparticles - A review. *Acta Biomaterialia*, *10*(10), 4023–4042. https://doi.org/10.1016/j.actbio.2014.05.022

Sharma, D., Kanchi, S., & Bisetty, K. (2019). Biogenic synthesis of nanoparticles: A review. *Arabian Journal of Chemistry*, *12*(8), 3576–3600. https://doi.org/10.1016/j.arabjc.2015.11.002

Silva, M. J., Gomes, J., Ferreira, P., & Martins, R. C. (2022). An Overview of Polymer-Supported Catalysts for Wastewater Treatment through Light-Driven Processes. *Water (Switzerland)*, *14*(5), 1–34. https://doi.org/10.3390/w14050825

Tripathi, S., Singh, V. K., Srivastava, P., Singh, R., Devi, R. S., Kumar, A., & Bhadouria, R. (2019). Phytoremediation of organic pollutants: Current status and future directions. In *Abatement of Environmental Pollutants: Trends and Strategies*. Elsevier Inc. https://doi.org/10.1016/B978-0-12-818095-2.00004-7

Vasiljevic, Z. Z., Dojcinovic, M. P., Vujancevic, J. D., Jankovic-Castvan, I., Ognjanovic, M., Tadic, N. B., Stojadinovic, S., Brankovic, G. O., & Nikolic, M. V. (2020). Photocatalytic degradation of methylene blue under natural sunlight using iron titanate nanoparticles prepared by a modified sol-gel method: Methylene blue degradation with Fe2TiO5. *Royal Society Open Science*, *7*(9). https://doi.org/10.1098/rsos.200708

Venkatesh, N. (2018). Metallic Nanoparticle: A Review. *Biomedical Journal of Scientific & Technical Research*, *4*(2), 3765–3775. https://doi.org/10.26717/bjstr.2018.04.0001011

Wang, J., Xu, J., & Wu, N. (2017). Kinetics and equilibrium studies of methylene blue adsorption on 2D nanolamellar Fe3O4. *Journal of Experimental Nanoscience*, *12*(1), 297–307. https://doi.org/10.1080/17458080.2017.1325016

Wang, S., & Gao, L. (2019). Laser-driven nanomaterials and laser-enabled nanofabrication for industrial applications. In *Industrial Applications of Nanomaterials*. Elsevier Inc. https://doi.org/10.1016/B978-0-12-815749-7.00007-4

Wu, W., He, Q., & Jiang, C. (2008). Magnetic iron oxide nanoparticles: Synthesis and surface functionalization strategies. *Nanoscale Research Letters*, *3*(11), 397–415. https://doi.org/10.1007/s11671-008-9174-9

Xu, C., Rangaiah, G. P., & Zhao, X. S. (2014). Photocatalytic degradation of methylene blue by titanium dioxide: Experimental and modeling study. *Industrial and Engineering Chemistry Research*, *53*(38), 14641–14649. https://doi.org/10.1021/ie502367x

Yaseen, D. A., & Scholz, M. (2019). Impact of pH on the Treatment of Artificial Textile Wastewater Containing Azo Dyes Using Pond Systems. *International Journal of Environmental Research*, *13*(2), 367–385. https://doi.org/10.1007/s41742-019-00180-1

Yew, Y. P., Shameli, K., Miyake, M., Kuwano, N., Bt Ahmad Khairudin, N. B., Bt Mohamad, S. E., & Lee, K. X. (2016). Green Synthesis of Magnetite (Fe3O4) Nanoparticles Using Seaweed (Kappaphycus alvarezii) Extract. *Nanoscale Research Letters*, *11*(1). https://doi.org/10.1186/s11671-016-1498-2

Zhang, J., Yu, Y., & Zhang, B. (2020). Synthesis and characterization of size controlled alloy nanoparticles. *Physical Sciences Reviews*, *5*(3), 1–19. https://doi.org/10.1515/psr-2018-0046

Zhang, X. F., Liu, Z. G., Shen, W., & Gurunathan, S. (2016). Silver nanoparticles: Synthesis, characterization, properties, applications, and therapeutic approaches. *International Journal of Molecular Sciences*, *17*(9). https://doi.org/10.3390/ijms17091534